Structural phase transition and spin state in the perovskite cobalt oxides $La_{1-x}Pr_xCoO_3$ ($x = 0.30, 0.34$)

Daisuke Urushihara,[1,*] Chie Ando,[1] Mai Komabuchi,[1] Koichiro Fukuda,[1] Yuki Nakahira,[2] Chikako Moriyoshi,[3] Shunsuke Kitou,[4] Nobuyuki Abe,[4,5] Taka-hisa Arima,[4] and Toru Asaka[1,†]

[1]*Division of Advanced Ceramics, Nagoya Institute of Technology, Nagoya 466-8555, Japan*

[2]*Foundational Quantum Technology Research Directorate, National Institutes for Quantum Science and Technology (QST), Hyogo 679-5148, Japan*

[3]*Graduate School of Advanced Science and Engineering, Hiroshima University, Higashihiroshima 739-8526, Japan*

[4]*Department of Advanced Materials Science, University of Tokyo, Kashiwa 277-8561, Japan*

[5]*Department of Physics, College of Humanity and Sciences, Nihon University, Tokyo 156-8550, Japan*

(Received 2 October 2023; accepted 5 January 2024; published 29 January 2024)

We investigated the correlation between crystal structures and spin states of cobalt perovskites $La_{1-x}Pr_xCoO_3$ ($x = 0.30, 0.34$) by x-ray powder diffraction, transmission electron microscopy, and magnetic measurements at low temperatures. The $x = 0.30$ and $x = 0.34$ compounds exhibit structural phase transitions between a low-temperature orthorhombic phase (*Pbnm*) and a high-temperature rhombohedral phase ($R\bar{3}c$) at around 170 and 250 K, respectively. In fairly wide temperature ranges around these temperatures, the low-temperature phase and the high-temperature phase coexist. The contribution of Co^{3+} ions to magnetic susceptibility approaches zero with decreasing temperatures. This indicates that low-spin cobalt ions increased at low temperatures. The CoO_6 octahedron in the low-temperature orthorhombic phase shows an almost isotropic one in low temperatures, but changes to an anisotropic one as the temperature rises until the phase transition temperature. This suggests that the intermediate-spin state gradually develops from the low-temperature dominant low-spin state with increasing temperature. We also observed small anomalies in the magnetic susceptibility of each compound in the vicinity of the structural phase transition temperature.

DOI: 10.1103/PhysRevB.109.024115

I. INTRODUCTION

$RCoO_3$ (R = rare-earth ions) is a typical perovskite-type compound showing a spin crossover [1]. This phenomenon arises from the competition between the ligand field energy and the intra-atomic Hund's exchange interaction. Namely, the spin state and orbital state strongly correlate in $RCoO_3$. Thus, the spin crossover occurs with the changes in the CoO_6 octahedral coordination environment by applying the external stimulus, such as temperature, stress, light irradiation, etc. [2–4]. At that time, Co^{3+} ions, which belong to the $3d^6$ electron configuration, can show three types of spin states: low- (t_{2g}^6, $S = 0$), intermediate- ($t_{2g}^5e_g^1$, $S = 1$), and high-spin ($t_{2g}^4e_g^2$, $S = 2$) states. Clarifying and controlling the spin state by several external fields attract remarkable attention.

$LaCoO_3$ is one of the most intensively studied compounds in the $RCoO_3$ series, because of its unique physical properties different from other $RCoO_3$ compounds. There are some differences in the crystal structure and physical properties between $LaCoO_3$ and $PrCoO_3$, owing to the different ionic radii of La and Pr ions, which are 1.216 and 1.179 Å in nine coordination, respectively [5]. With respect to the magnetic properties, $LaCoO_3$ exhibits spin crossover at two temperatures around 100 and 500 K [6]. However, $PrCoO_3$ exhibits spin crossover only at around 500 K [7–9]. Regarding the crystal structure at room temperature, $LaCoO_3$ has the trigonal $R\bar{3}c$ structure [10], while $PrCoO_3$ has the orthorhombic *Pbnm* one [11], as shown in Fig. 1. These phases have different octahedral tilts and degrees of freedom of bond lengths and angles. With respect to the relation to the octahedral coordination, the CoO_6 octahedra cooperatively tilt in the manner of $a^-a^-a^-$ in $LaCoO_3$, while they tilt in the manner of $a^-a^-c^+$ in $PrCoO_3$, using the Glazer notation [12]. Therefore, the network structure of CoO_6 octahedra and the coordination environment of Co^{3+} ions in these compounds are different from each other. $RCoO_3$ compounds except $LaCoO_3$ are subject to the orthorhombic distortion at low temperatures.

In order to obtain knowledge on changes in physical properties by changing the ionic radius of the A-site ions, the solid solution compounds $La_{1-x}Pr_xCoO_3$ have been paid a lot of attention. According to the reported phase diagram, the space group at room temperature is trigonal $R\bar{3}c$ for $0 \leqslant x \leqslant 0.3$ and orthorhombic *Pbnm* for $0.7 \leqslant x \leqslant 1$ [13–15]. The composition between $x = 0.3$ and 0.7 has been described as a mixture state of the $R\bar{3}c$ and *Pbnm* phases. In the small Pr-content range of $x \leqslant 0.3$, the magnetic susceptibility shows a similar tendency to that of $LaCoO_3$, where the magnetic susceptibility of the Co^{3+} ions shows a broad maximum between 100 and 200 K and reaches zero with decreasing the temperature [13,15].

The first magnetic excited state above 100 K in $LaCoO_3$ was thought to be a contribution of a high-spin state from

*urushihara.daisuke@nitech.ac.jp
†asaka.toru@nitech.ac.jp

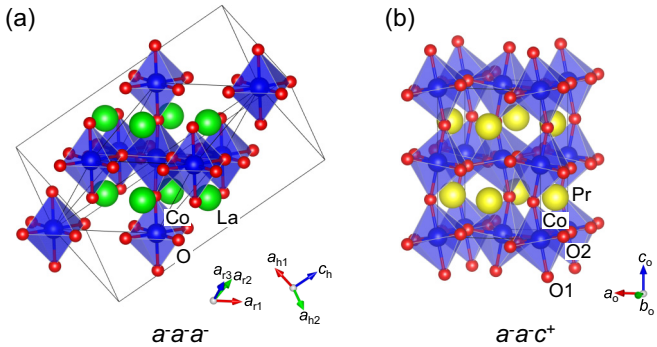

FIG. 1. Crystal structures of (a) $LaCoO_3$ and (b) $PrCoO_3$. Green, yellow, blue, and red spheres denote La, Pr, Co, and O, respectively.

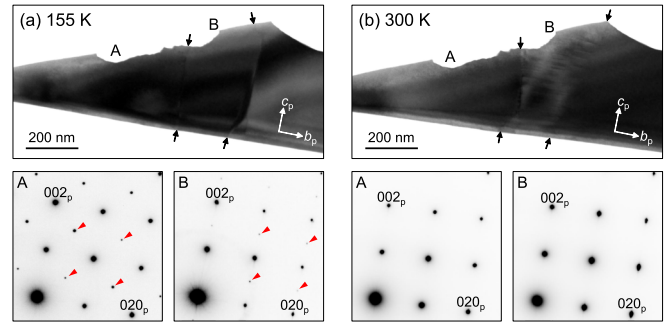

FIG. 2. TEM images of $La_{0.70}Pr_{0.30}CoO_3$ at (a) 155 K and (b) 300 K. $[100]_p$-zone axis SAED patterns of regions A and B. Black arrows in TEM images indicate an edge of twin boundaries. Red triangles in (a) indicate superstructure reflections for the simple cubic perovskite structure.

the experimental and theoretical results [16–20]. This state was explained as an inhomogeneous mixed-spin state system caused by a low-spin ground state and a high-spin excited state. The high-spin state with $S = 2$ has, in a cubic crystal-field, the occupation $t_{2g}^4 e_g^2$, which can be described by an effective orbital moment $\tilde{L} = 1$ [21]. Spin-orbit coupling (SOC) splits this state into the lowest-lying triplet and the other two states. Considering the high-spin triplet state split by the trigonal crystal field and SOC, a g factor of 3.35 obtained from electron spin resonance [17] and inelastic neutron scattering data [20] was well described. In contrast, the intermediate-spin state for the phase was argued in some previous studies [6,22–25]. Since the intermediate-spin state of Co^{3+} is Jahn-Teller (JT) active, there should be anisotropies of bond lengths in each CoO_6 octahedron, when the intermediate-spin state is stable. It was reported that the structure of the thermally equilibrium phase of $LaCoO_3$ above 100 K was not trigonal $R\bar{3}c$ without the JT distortion which is involved with e_g orbitals, but monoclinic $I2/a$ with such JT distortion from diffraction experiments [24] and x-ray absorption spectroscopy [25]. In the rhombohedrally distorted perovskite of $R\bar{3}c$ symmetry all the Co-O bonds are identical. It is hence proposed that the space group $I2/a$ is thought of as evidence of the intermediate-spin state with spin crossover. However, because of few changes in lattice distortion, $LaCoO_3$ at room temperature is still thought of as $R\bar{3}c$ but $I2/a$ in some previous studies [13,15]. In short, it is still controversial whether the low-spin ground state changes to the high- or intermediate-spin states across the spin crossover in $RCoO_3$.

From the crystallographic point of view, the crystal structure and phase transition at the morphotropic phase boundary of $La_{1-x}Pr_xCoO_3$ are interesting because the end member structures of $LaCoO_3$ and $PrCoO_3$ have contrasting structural distortions. According to the reported phase diagram [13], around $x = 0.30$, the crystal structure shows $R\bar{3}c$ and almost the phase boundary between the single-phase state and the coexistence state of $R\bar{3}c$ and $Pbnm$ phases. CoO_6 octahedra in the $R\bar{3}c$ structure do not have typical JT distortion, while those in the $Pbnm$ structure can be accompanied with such JT distortion. In this study, we perform a magnetic susceptibility measurement and a crystal structure analysis using x-ray powder diffraction (XRPD) and transmission electron microscopy (TEM) to obtain the information about the correlation between the crystal structure and the spin-crossover phenomenon in this system.

II. EXPERIMENT

Single crystals were grown by the floating-zone method. The reagents of La_2O_3, Pr_6O_{11}, and Co_3O_4 were weighed in stoichiometric proportions of $La_{1-x}Pr_xCoO_3$ ($x = 0.30, 0.34$) and then ground together to form a mixture. The mixture was calcined at 1273 K for 12 h, pressed into a 3 mmϕ × 100 mm rod, and then sintered at 1573 K for 24 h. A black crystal block was grown in 5 atm oxygen gas with a feed rate of 1.0–1.5 mm/h.

For the TEM observation, single crystals were thinned by mechanical grinding and Ar^+ ion beam milling. We performed the selected area electron diffraction (SAED) and bright-field (BF) imaging with a JEM-ARM200F (JEOL), operated at 200 kV. The temperature profile of SAED patterns and BF images were obtained with increasing temperature after cooling to 155 K using a cooling TEM holder.

The XRPD patterns were obtained at beamline BL02B2 of the SPring-8 synchrotron facility [26,27]. Powder specimens were ground and placed in borosilicate capillaries with a diameter of ϕ200 μm. The diffraction data were collected in Debye-Scherrer geometry with an x-ray beam of wavelength $\lambda = 0.499888(1)$ Å. The sample temperature was controlled in the temperature range 100–400 K by using a nitrogen spray device. The structural parameters were refined by the Rietveld method using the program RIETAN-FP [28]. We fixed the occupation factors of La and Pr at the rare-earth site to the nominal chemical compositions.

The magnetization measurements were performed using a magnetic property measurement system (MPMS, Quantum Design). The data were obtained between 5 and 400 K during heating and cooling processes.

III. RESULTS AND DISCUSSION

Figure 2 shows TEM images and SAED patterns of an $x = 0.30$ sample. The curved lines between black arrows in the TEM images correspond to twin boundaries. The SAED patterns for two twin variants separated by the twin boundary

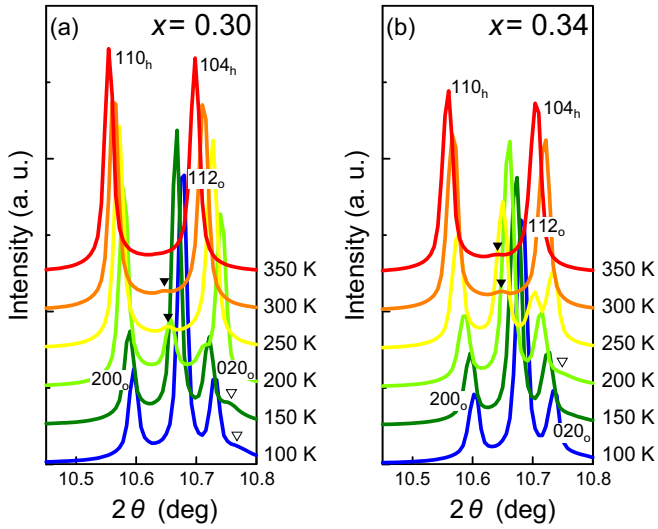

FIG. 3. Temperature evolution of XRD patterns in (a) $La_{0.70}Pr_{0.30}CoO_3$ and (b) $La_{0.66}Pr_{0.34}CoO_3$. Filled and open triangles indicate peaks of the residual low- and high-temperature phases, respectively.

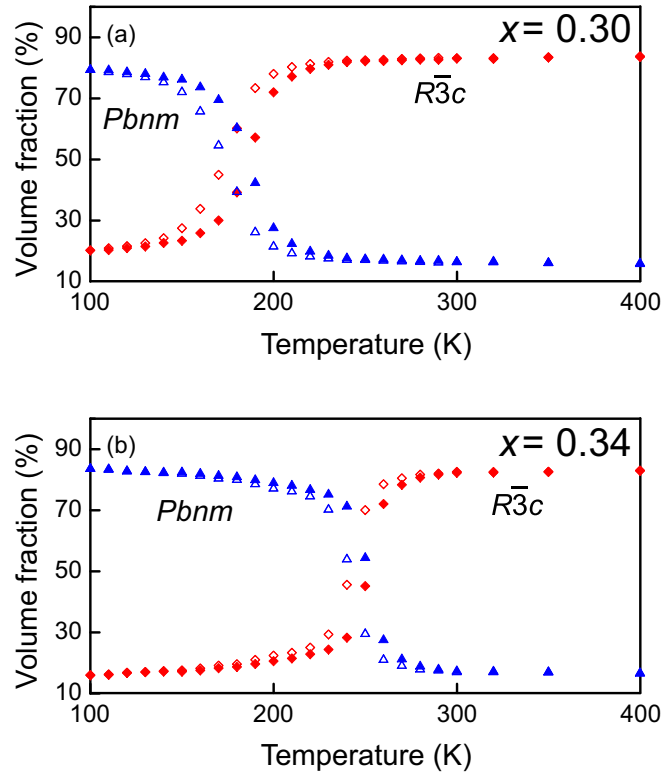

FIG. 4. Temperature dependence of volume fractions of the two phases estimated by Rietveld analysis in (a) $La_{0.70}Pr_{0.30}CoO_3$ and (b) $La_{0.66}Pr_{0.34}CoO_3$. Filled and open symbols indicate the data collected in heating and cooling processes, respectively.

are clearly different at both 155 and 300 K. As indicated by red arrows in Fig. 2(a), the (0 1/2 1/2) and (0 0 1/2) types of superstructure reflections are observed in the SAED pattern for the variants A and B, respectively. The reflection indices in Fig. 2 are represented in the lattice setting of a simple cubic perovskite structure. Based on a careful analysis of SAED patterns, we assign the space group at 155 K to the orthorhombic *Pbnm*. The monoclinic $I2/a$ structure, which was reported as the phase with the intermediate-spin state in $LaCoO_3$ [24], is excluded from the extinction rule. The variants A and B are related by a 90° rotation [Fig. 2(a)]. On the other hand, this compound has the trigonal (rhombohedral) $R\bar{3}c$ symmetry at 300 K [29], which is consistent with some previous reports [13–15]. The variants A and B in the rhombohedral phase show almost the same diffraction patterns [Fig. 2(b)]. They maintain the relationship of 90° rotational twins in the $R\bar{3}c$ structure. They can be regarded as ferroelastic domain structures which are formed by breaking the fourfold symmetry of the aristotype simple cubic perovskite structure [30,31]. Slight differences in the position of the twin boundaries between the low-temperature orthorhombic and high-temperature rhombohedral phases are observed. This twin boundary displacement is a manifestation of the (ferro)elastic nature of this compound.

The structural phase transitions are also confirmed by XRPD. Figures 3(a) and 3(b) show the temperature evolution of XRPD for $La_{0.70}Pr_{0.30}CoO_3$ and $La_{0.66}Pr_{0.34}CoO_3$, respectively. The reflection indices for the rhombohedral and orthorhombic phases are based on the hexagonal and orthorhombic unit cells and are attached with subscripts h and o, respectively. In the cooling process, the 104_h reflection decreases in intensity and shifts to a higher angle, while 112_o and 020_o reflections appear in the profile in both compounds. Both the compounds show a phase coexistence, which signifies a first-order structural phase transition. As indicated by the filled and open triangles in Fig. 3, the two phases coexist in a fairly wide temperature range. In $La_{0.70}Pr_{0.30}CoO_3$, the high-temperature rhombohedral phase remains down to 100 K and the low-temperature phase remains up to 300 K, although the transition temperature is ∼170 K in the cooling process (see Fig. 4). The coexistence in a wide temperature range is also observed in $La_{0.66}Pr_{0.34}CoO_3$ indicating that the phase coexistence is essential at the vicinity of morphotropic phase boundary in the $La_{1-x}Pr_xCoO_3$ system.

The low-temperature phase of $LaCoO_3$, which shows the phase transition between cubic and trigonal systems, was reported to have ferroelasticity with multidomain structures due to trigonal distortion [30]. The ferroelastic behavior is also expected in the crystals prepared in the present study, which have multidomain structures, as shown in Fig. 2. The multidomain structure in the $La_{1-x}Pr_xCoO_3$ system seems to be more complex than that of $LaCoO_3$, because of the transition between trigonal and orthorhombic phases. The first-order structural phase transition in $La_{1-x}Pr_xCoO_3$ between $R\bar{3}c$ and *Pbnm*, including the opposite octahedral rotation from the $a^-a^-a^-$ to $a^-a^-c^+$ manner, accompanies a volume change (see Fig. 5). The first-order structural phase transition must produce local strain, especially in a multidomain state. The diffuse structural phase transition observed in the XRPD would be due to a distribution of internal stress by structural phase transitions that occur locally and ubiquitously in the initial stage of phase transition. The residual local strain due to volume changes and multidomain structures would cause the diffuse phase transition in the $La_{1-x}Pr_xCoO_3$ system.

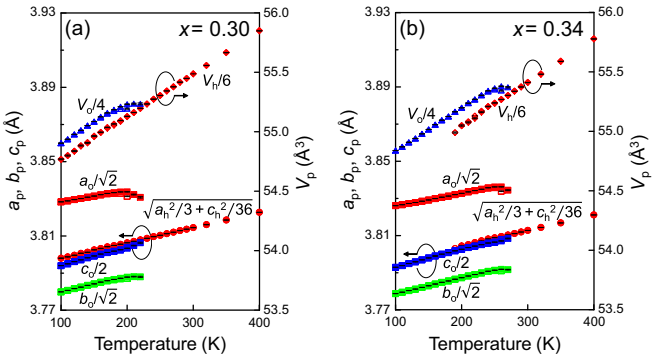

FIG. 5. Temperature dependence of lattice constants and unit-cell volumes in (a) $La_{0.70}Pr_{0.30}CoO_3$ and (b) $La_{0.66}Pr_{0.34}CoO_3$. Filled and open symbols indicate the data collected in heating and cooling process, respectively.

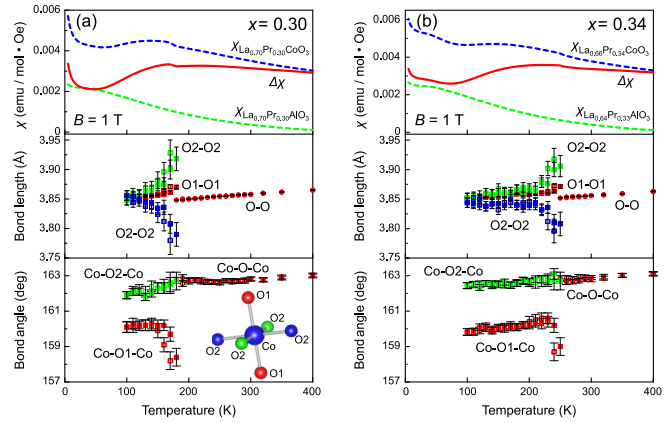

FIG. 6. Temperature dependence of magnetic susceptibility, diagonal O-O bond lengths and Co-O-Co bond angles of CoO_6 octahedron in (a) $La_{0.70}Pr_{0.30}CoO_3$ and (b) $La_{0.66}Pr_{0.34}CoO_3$. Filled and open symbols indicate the data collected in the heating and cooling processes, respectively. The colors of O-O bond lengths correspond to the oxygen colors in the octahedron inserted.

The volume fractions of the high-temperature rhombohedral and low-temperature orthorhombic phases at each temperature estimated by the Rietveld analysis are shown in Fig. 4. The minority-phase fraction exceeds 10% in the whole measured temperature range. These results correspond to a few peaks in Figs. 3 and Supplemental Material S1 [32]. The structural phase transition between the rhombohedral ($R\bar{3}c$) and orthorhombic ($Pbnm$) phases in $LaCo_{1-x}Fe_xO_3$ and $La_{1-x}Sm_xGaO_3$ shows similar diffuse phase transitions [33,34]. The structural changes in $La_{1-x}Sm_xGaO_3$ occur in the temperature range 640–840 K. These phenomena also would be due to the first-order phase transition and ferroelastic behavior.

Figure 5 shows the temperature dependence of lattice constants of $La_{0.70}Pr_{0.30}CoO_3$ and $La_{0.66}Pr_{0.34}CoO_3$. Here, $a_p = \sqrt{a_h^2/3 + c_h^2/36}$ and $a_p = a_o/\sqrt{2}$, $b_p = b_o/\sqrt{2}$, $c_p = c_o/2$ for the high-temperature rhombohedral and low-temperature orthorhombic phases, respectively. These formulas are derived from the geometry of the primitive perovskite unit cell, which corresponds with the nearest neighbor Co-Co distance, as shown in Fig. S2 [32]. The high-temperature rhombohedral phase has one kind of the Co-Co distance, while the low-temperature orthorhombic phase shows three kinds. Although a small amount of residual phase exists for a wide temperature range, the lattice constants of the phase whose volume fraction is less than 20% are not plotted in Fig. 5 because of a low accuracy.

The cell volume for each chemical composition is also plotted in Fig. 5 as a function of temperature. Near the phase transition temperature, we observe a jump and thermal hysteresis of the volume as well as the lattice constants in the heating and cooling processes, indicating again the first-order nature of the phase transition. Since the space groups $R\bar{3}c$ and $Pbnm$ are not of group-subgroup relation, the phase transition between them should be of the first order. The thermal hysteresis and phase coexistence phenomena make the phase boundary on the phase diagram complicated. The solid-solution range of $La_{1-x}Pr_xCoO_3$ is wider than that of the previous reports [13–15], or $La_{1-x}Pr_xCoO_3$ may be an all-proportional solid solution system.

Figure 6 shows the temperature dependence of the magnetic susceptibility of $La_{1-x}Pr_xCoO_3$ and $La_{1-x}Pr_xAlO_3$, along with the difference $\Delta\chi(T)$. To show the contribution of Co^{3+}, we subtract the contribution of Pr^{3+} using the magnetic susceptibility of $La_{0.70}Pr_{0.30}AlO_3$ from that of $La_{0.70}Pr_{0.30}CoO_3$. Here, the magnetic susceptibility of $La_{0.66}Pr_{0.34}AlO_3$ was calculated from $La_{0.70}Pr_{0.30}AlO_3$ by multiplying. In the $x = 0.30$ compound, with decreasing temperature from 400 K, the magnetic susceptibility $\Delta\chi(T)$ decreases after the maximum at ~150 K. With further cooling, it turns to an upward trend at 50 K. This phenomenon is likely due to the Pr-4f state of $La_{1-x}Pr_xCoO_3$ at low temperatures different from the ordinary localized 4f state due to the hybridization between the Pr-4f and Co-3d states [13,35]. Even after subtracting the contribution of $La_{1-x}Pr_xAlO_3$, $\Delta\chi(T)$ includes the contribution of Co^{3+} and Pr^{3+}. $\Delta\chi(T)$ of the $x = 0.30$ compound shows a small jump at ~170 K. A similar jump is observed at ~250 K in the $x = 0.34$ compound. The observed small jumps are obviously related to the structural phase transition.

The diagonal O-O bond lengths in $La_{1-x}Pr_xCoO_3$ represent the distortion of CoO_6 octahedron, which is strongly related to the spin state in Co^{3+}. The colors of O-O bond lengths in Fig. 6 correspond to the oxygen colors in the octahedron inserted in Fig. 6(a). The low-spin and the high-spin states in Co^{3+} are expected to show almost the same O-O bond lengths due to the electron configuration in e_g and t_{2g} orbitals. The low-spin state shows perfectly isotropic O-O bond lengths due to the orbital configuration of $t_{2g}^6 e_g^0$. In the high-spin state, small distortion of the CoO_6 octahedron appears because of the orbital configuration of $t_{2g}^4 e_g^2$. By contrast, the intermediate-spin state would show larger octahedral distortion of elongation/compression type due to the orbital configuration of $t_{2g}^5 e_g^1$, that is the JT distortion. In Fig. 6(b), three independent diagonal O-O bond lengths of $La_{0.66}Pr_{0.34}CoO_3$ below the phase transition temperature are almost the same values between 100 and 200 K despite the degree of freedom of the bond lengths within the octahedron in the orthorhombic $Pbnm$ structure. Co^{3+} in $RCoO_3$ is assumed to have the low-spin state as the ground state at low

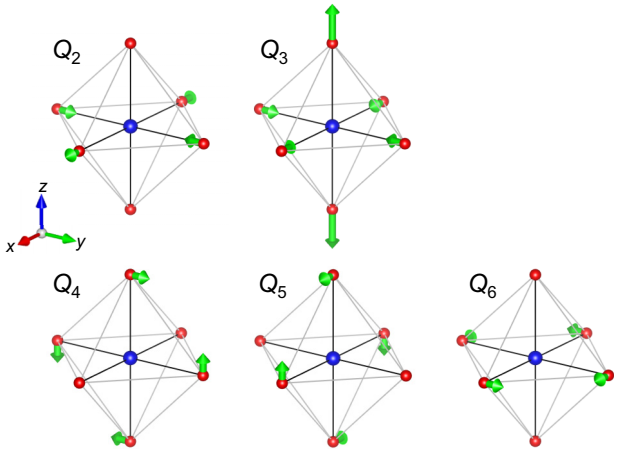

FIG. 7. Schematic illustration of the Q_2 and Q_3 (E_g) and the Q_4, Q_5, and Q_6 (T_{2g}) modes of an octahedron.

temperatures [7,13]. Therefore, we conclude that this isotropic bond length reflects the low-spin state. This is consistent with the behavior of $\Delta\chi(T)$ at low temperatures. In contrast, the anisotropy of O-O bond lengths increases gradually, when the temperature is raised and approaches the phase transition temperature. One of the three bonds shrinks, the other two elongate, and Co-O-Co bond angles also change, as shown in Fig. 6. In the high-temperature phase, the O-O bond lengths become isotropic again due to the constraints of crystal symmetries.

In order to discuss the octahedral distortion quantitively, we analyzed the distortion of the CoO_6 octahedra. In the Co^{3+} ion in the CoO_6 octahedron, the orbital degree of freedom can interact with E_g (Q_2, Q_3) and T_{2g} (Q_4, Q_5, Q_6) modes [36,37]. The Q_2 and Q_3 modes are orthorhombic and tetragonal distortions, respectively, and the Q_4-Q_6 modes correspond to the deviation of the O-Co-O angle from 90° (Fig. 7). The linear combination of the T_{2g} (Q_4, Q_5, Q_6) modes produces the trigonal distortion Q_t as expressed by $Q_t = (Q_4 + Q_5 + Q_6)/\sqrt{3}$, which corresponds to the elongation or compression along one of the four $\langle 111\rangle_c$ directions. Figures 8(a) and 8(c) show the distortion of CoO_6 octahedra in the Q_2-Q_3 plane for $x = 0.30$ and 0.34, respectively. In the Q_2-Q_3 plane of the $x = 0.30$, the Q_2 mode is dominant rather than the Q_3 mode between 100 K and the phase transition temperature of 170 K. At 100 K, the distortion of the E_g mode is considerably smaller and represents the isotropic octahedron, indicating the low-spin state of $t_{2g}^6 e_g^0$. With increasing temperature, the distortion of the E_g mode increases until the phase transition temperature of 170 K, as shown in Fig. 8(b). Therefore, the population of the intermediate-spin state increases rather than the high-spin state, because the intermediate-spin state has the orbital degree of freedom of the E_g mode but the high-spin state does not.

In the high-temperature phase, the distortion of the E_g mode disappears due to symmetrical constraints of the $R\bar{3}c$ structure. Q_t shows the compressed trigonal distortion along the $[001]_h$ direction, which corresponds to the [111] direction in the simple cubic perovskite basis, accompanied by the level splitting of t_{2g} orbital to a_{1g} and doubly degenerate e'_g orbitals

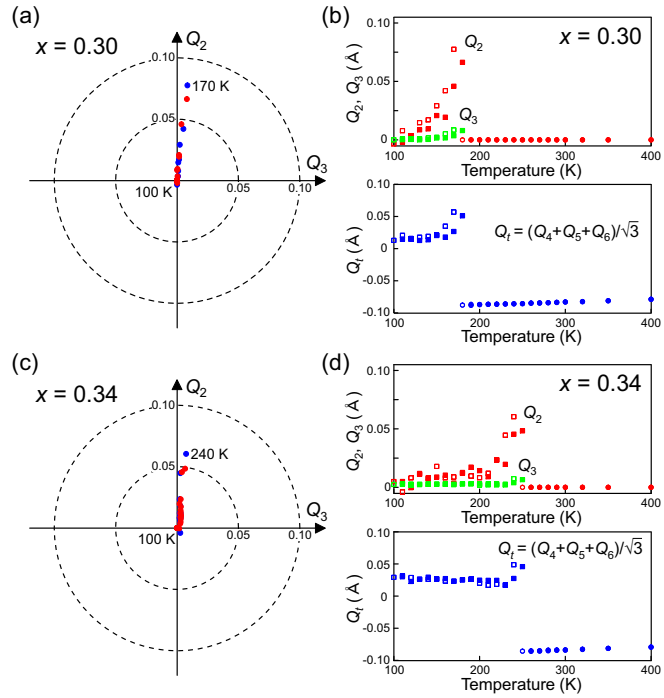

FIG. 8. Q_2-Q_3 mode analysis and temperature dependence of the E_g (Q_2, Q_3) mode and trigonal distortion Q_t of CoO_6 octahedron in (a),(b) $La_{0.70}Pr_{0.30}CoO_3$ and (c),(d) $La_{0.66}Pr_{0.34}CoO_3$. Filled and open symbols indicate the data collected in the heating and cooling processes, respectively.

[38,39]. These phenomena are also observed in the compound of $x = 0.34$, as shown in Fig. 8(d). In the compressed trigonal distortion, the level of the a_{1g} orbital is lower than that of the e'_g one, based on the crystal field theory [40,41]. And, the compressed trigonal distortion is stable when the orbital configuration is t_{2g}^1 or t_{2g}^4, indicating that the high-spin state of $t_{2g}^4 e_g^2$ is suitable. By contrast, it was reported that the levels of the a_{1g} and e'_g orbitals are opposite by the $t_{2g}-e_g$ hybridization [42]. Namely, the intermediate-spin state of $t_{2g}^5 e_g^1$ would have the compressed trigonal distortion. From the Q_t mode, it is difficult to determine the spin state because of the complex contributions affecting the levels of the a_{1g} and e'_g orbitals. Furthermore, as an example of MO_6 octahedra with the compressed trigonal distortion, we cite the rhombohedral phase of the perovskite-type manganese oxide $La_{0.8}Sr_{0.2}MnO_{2.9}$ that has the orbital configuration of $t_{2g}^3 e_g^1$ [43]. This compound has been reported to have the octahedra with a compressed trigonal distortion similar to the high-temperature phase of $La_{1-x}Pr_xCoO_3$, although Mn^{3+} ions have orbital degree of freedom of E_g modes but not that of the T_{2g} modes. Such a distorted octahedron is different from the typical JT distortion, but may be compatible with the intermediate-spin state where one electron is accommodated in the e_g orbital in Co^{3+}. As a result, the structural analysis cannot rule out both possibilities of the intermediate- and high-spin states in the high-temperature $R\bar{3}c$ phase, although the low-temperature *Pbnm* phase indicates the spin crossover between the low- and intermediate-spin states.

IV. CONCLUSIONS

The crystal structures of $La_{1-x}Pr_xCoO_3$ ($x = 0.30$, 0.34) are determined using synchrotron radiation x-ray powder diffraction over a broad range of temperatures. The space groups of the high- and low-temperature phases are determined to be $R\bar{3}c$ and *Pbnm*, which are the same space group as the end-member compounds $LaCoO_3$ and $PrCoO_3$, respectively. Both compounds show a wide range coexistence of the high- and low-temperature phases, which is not chemical phase separation but diffuse structural phase transition. The composition-crystal structure phase diagram with the end members of $LaCoO_3$ and $PrCoO_3$ reported so far [13], which are described as discontinuous solid solutions, is suggested to be revised. The magnetic susceptibility of Co^{3+} in $La_{1-x}Pr_xCoO_3$ ($x = 0.30$, 0.34) shows a small jump at the structural phase transition temperature. The diagonal O-O bond lengths in CoO_6 octahedra at low temperatures are almost the same in spite of having the degree of freedom of O-O bond lengths, indicating the low-spin state. In contrast, the observed anisotropic O-O bond lengths suggest that Co^{3+} is in the intermediate-spin state with the distortion of the Q_2 mode in the low-temperature *Pbnm* phase.

ACKNOWLEDGMENTS

The XRD measurements were performed at the BL02B2 beamline of SPring-8 with the approval of the Japan Synchrotron Radiation Research Institute (Proposal No. 2018B1699). The crystal structure is visualized using the program VESTA [44]. This work was partly supported by JSPS KAKENHI Grants No. 21K04641 and No. 21K03431 and "Advanced Research Infrastructure for Materials and Nanotechnology in Japan (ARIM)" of the Ministry of Education, Culture, Sports, Science and Technology (MEXT), Grants No. JPMXP1222NI0108 and No. JPMXP1223NI0106.

[1] J. Kuneš and V. Křápek, Disproportionation and metallization at low-spin to high-spin transition in multiorbital mott systems, Phys. Rev. Lett. **106**, 256401 (2011).

[2] G. Vankó, J. P. Rueff, A. Mattila, Z. Németh, and A. Shukla, Temperature- and pressure-induced spin-state transitions in $LaCoO_3$, Phys. Rev. B **73**, 024424 (2006).

[3] J. Fujioka, Y. Yamasaki, A. Doi, H. Nakao, R. Kumai, Y. Murakami, M. Nakamura, M. Kawasaki, T. Arima, and Y. Tokura, Strain-sensitive spin-state ordering in thin films of perovskite $LaCoO_3$, Phys. Rev. B **92**, 195115 (2015).

[4] Y. Okimoto, X. Peng, M. Tamura, T. Morita, K. Onda, T. Ishikawa, S. Koshihara, N. Todoroki, T. Kyomen, and M. Itoh, Ultrasonic propagation of a metallic domain in $Pr_{0.5}Ca_{0.5}CoO_3$ undergoing a photoinduced insulator-metal transition, Phys. Rev. Lett. **103**, 027402 (2009).

[5] R. D. Shannon, Revised effective ionic radii and systematic studies of interatomic distances in halides and chalcogenides, Acta Crystallogr., Sect. A **32**, 751 (1976).

[6] K. Asai, A. Yoneda, O. Yokokura, J. M. Tranquada, G. Shirane, and K. Kohn, Two spin-state transitions in $LaCoO_3$, J. Phys. Soc. Jpn. **67**, 290 (1998).

[7] G. Thornton, F. C. Morrison, S. Partington, B. C. Tofield, and D. E. Williams, The rare earth cobaltates: Localised or collective electron behaviour? J. Phys. C **21**, 2871 (1988).

[8] M. Itoh, M. Mori, S. Yamaguchi, and Y. Tokura, NMR study of the spin state of $RCoO_3$ (R = Pr, Nd, Sm, and Eu), Phys. B (Amsterdam, Neth.) **259-261**, 902 (1999).

[9] M. Itoh, J. Hashimoto, S. Yamaguchi, and Y. Tokura, Spin state and metal–insulator transition in $LaCoO_3$ and $RCoO_3$ (R = Nd, Sm and Eu), Phys. B (Amsterdam, Neth.) **281-282**, 510 (2000).

[10] G. Thornton, B. C. Tofield, and A. W. Hewat, A neutron diffraction study of $LaCoO_3$ in the temperature range $4.2 < T < 1248$ K, J. Solid State Chem. **61**, 301 (1986).

[11] X. Liu and C. T. Prewitt, High-temperature diffraction study of $LnCoO_3$ perovskites: A high-order electronic phase transition, J. Phys. Chem. Solids **52**, 441 (1991).

[12] A. M. Glazer, The classification of tilted octahedra in perovskites, Acta Crystallogr., Sect. B **28**, 3384 (1972).

[13] Y. Kobayashi, T. Mogi, and K. Asai, Spin-state transition in $La_{1-x}Pr_xCoO_3$, J. Phys. Soc. Jpn. **75**, 104703 (2006).

[14] O. Myakush, V. Berezovets, A. Senyshyn, and L. Vasylechko, Preparation and crystal structure of new perovskite-type cobaltites $R_{1-x}R'_xCoO_3$, Chem. Met. Alloys **3**, 184 (2010).

[15] A. S. Panfilov, A. A. Lyogenkaya, G. E. Grechnev, V. A. Pashchenko, L. O. Vasylechko, V. M. Hreb, and A. V. Kovalevsky, Effects of temperature and pressure on the magnetic properties of $La_{1-x}Pr_xCoO_3$, Phys. Status Solidi B **257**, 2000085 (2020).

[16] J. B. Goodenough, An interpretation of the magnetic properties of the perovskite-type mixed crystals $La_{1-x}Sr_xCoO_{3-\lambda}$, J. Phys. Chem. Solids **6**, 287 (1958).

[17] S. Noguchi, S. Kawamata, K. Okuda, H. Nojiri, and M. Motokawa, Evidence for the excited triplet of Co3+ in $LaCoO_3$, Phys. Rev. B **66**, 094404 (2002).

[18] Z. Ropka and R. J. Radwanski, ^5D term origin of the excited triplet in $LaCoO_3$, Phys. Rev. B **67**, 172401 (2003).

[19] M. W. Haverkort, Z. Hu, J. C. Cezar, T. Burnus, H. Hartmann, M. Reuther, C. Zobel, T. Lorenz, A. Tanaka, N. B. Brookes, H. H. Hsieh, H.-J. Lin, C. T. Chen, and L. H. Tjeng, Spin state transition in $LaCoO_3$ studied using soft x-ray absorption spectroscopy and magnetic circular dichroism, Phys. Rev. Lett. **97**, 176405 (2006).

[20] A. Podlesnyak, S. Streule, J. Mesot, M. Medarde, E. Pomjakushina, K. Conder, A. Tanaka, M. W. Haverkort, and D. I. Khomskii, Spin-state transition in $LaCoO_3$: Direct neutron spectroscopic evidence of excited magnetic states, Phys. Rev. Lett. **97**, 247208 (2006).

[21] A. Abragham and B. Bleaney, *Electron Paramagnetic Resonance of Transition Ions* (Clarendon, Oxford, 1970).

[22] M. A. Korotin, S. Yu. Ezhov, I. V. Solovyev, V. I. Anisimov, D. I. Khomskii, and G. A. Sawatzky, Intermediate-spin state and properties of $LaCoO_3$, Phys. Rev. B **54**, 5309 (1996).

[23] S. Yamaguchi, Y. Okimoto, and Y. Tokura, Local lattice distortion during the spin-state transition in $LaCoO_3$, Phys. Rev. B **55**, 8666(R) (1997).

[24] G. Maris, Y. Ren, V. Volotchaev, C. Zobel, T. Lorenz, and T. T. M. Palstra, Evidence for orbital ordering in $LaCoO_3$, Phys. Rev. B **67**, 224423 (2003).

[25] O. Haas, R. P. W. J. Struis, and J. M. McBreen, Synchrotron x-ray absorption of $LaCoO_3$ perovskite, J. Solid State Chem. **177**, 1000 (2004).

[26] E. Nishibori, M. Takata, K. Kato, M. Sakata, Y. Kubota, S. Aoyagi, Y. Kuroiwa, M. Yamakata, and N. Ikeda, The large Debye–Scherrer camera installed at SPring-8 BL02B2 for charge density studies, Nucl. Instrum. Methods Phys. Res. **467-468**, 1045 (2001).

[27] S. Kawaguchi, M. Takemoto, K. Osaka, E. Nishibori, C. Moriyoshi, Y. Kubota,Y. Kuroiwa, and K. Sugimoto, High-throughput powder diffraction measurement system consisting of multiple MYTHEN detectors at beamline BL02B2 of SPring-8, Rev. Sci. Instrum. **88**, 085111 (2017).

[28] F. Izumi and K. Momma, Three-dimensional visualization in powder diffraction, Solid State Phenom. **130**, 15 (2007).

[29] No monoclinic-derived twin structure is observed in the TEM image taken over a wide area, and no clear reflection splitting or broadening is observed in the SAED or XRPD patterns. The possibility that the high-temperature phase is the monoclinic $I2/a$ is ruled out.

[30] N. Orlovskaya, N. Browning, and A. Nicholls, Ferroelasticity in mixed conducting $LaCoO_3$ based perovskites: A ferroelastic phase transition, Acta Mater. **51**, 5063 (2003).

[31] Y. Kobayashi, T. Mitsunaga, G. Fujinawa, T. Arii, M. Suetake, K. Asai, and J. Harada, Structural phase transition from rhombohedral to cubic in $LaCoO_3$, J. Phys. Soc. Jpn. **69**, 3468 (2000).

[32] See Supplemental Material at http://link.aps.org/supplemental/10.1103/PhysRevB.109.024115 for crystal data and structural parameters of $La_{1-x}Pr_xCoO_3$.

[33] D. V. Karpinsky, I. O. Troyanchuk, K. Bärner, H. Szymczak, and M. Tovar, Crystal structure and magnetic ordering of the $LaCo_{1-x}Fe_xO_3$ system, J. Phys.: Condens. Matter **17**, 7219 (2005).

[34] L. Vasylechko, R. Niewa, H. Borrmann, M. Knapp, D. Savytskii, A. Matkovski, U. Bismayer, and M. Berkowski, *R*-3*c*−*Pbnm* phase transition of $La_{1-x}Sm_xGaO_3$ ($0 < x < 0.3$) perovskites and crystal structures of the orthorhombic and trigonal phases, Solid State Ionics **143**, 219 (2001).

[35] Y. Kobayashi, Y. Terakado, and K. Asai, Change in Pr-4f ground state in $Pr_{1-x}Y_xCoO_3$, J. Phys. Soc. Jpn. **83**, 104704 (2014).

[36] U. Öpik and M. H. L. Pryce, Studies of the Jahn-Teller effect. I. A survey of the static problem, Proc. R. Soc. London, Ser. A **238**, 425 (1957).

[37] Y. Nii, H. Sagayama, T. Arima, S. Aoyagi, R. Sakai, S. Maki, E. Nishibori, H. Sawa, K. Sugimoto, H. Ohsumi, and M. Takata, Orbital structures in spinel vanadates AV_2O_4 (A = Fe, Mn), Phys. Rev. B **86**, 125142 (2012).

[38] M. Mochizuki, Y. Yanase, and M. Ogata, Ferromagnetic and triplet-pairing instabilities controlled by trigonal distortion of CoO_6 octahedra in $Na_xCoO_2 \cdot yH_2O$, J. Phys. Soc. Jpn. **74**, 1670 (2005).

[39] F. Rodolakis, J.-P. Rueff, M. Sikora, I. Alliot, J.-P. Itié, F. Baudelet, S. Ravy, P. Wzietek, P. Hansmann, A. Toschi, M. W. Haverkort, G. Sangiovanni, K. Held, P. Metcalf, and M. Marsi, Evolution of the electronic structure of a Mott system across its phase diagram: X-ray absorption spectroscopy study of $(V_{1-x}Cr_x)_2O_3$, Phys. Rev. B **84**, 245113 (2011).

[40] W. Koshibae and S. Maekawa, Electronic state of a CoO_2 layer with hexagonal structure: A kagomé lattice structure in a triangular lattice, Phys. Rev. Lett. **91**, 257003 (2003).

[41] S. V. Streltsov, F. V. Temnikov, K. I. Kugel, and D. I. Khomskii, Interplay of the Jahn-Teller effect and spin-orbit coupling: The case of trigonal vibrations, Phys. Rev. B **105**, 205142 (2022).

[42] S. Landron and M. B. Lepetit, Importance of t_{2g}-e_g hybridization in transition metal oxides, Phys. Rev. B **77**, 125106 (2008).

[43] T. Mori, K. Inoue, and N. Kamegashira, Phase behavior in the system $La_xSr_{1-x}MnO_{(5+x)/2}$ ($x = 0.8-1.0$) with trivalent state of manganese ion, J. Alloys Compd. **308**, 87 (2000).

[44] K. Momma and F. Izumi, *VESTA3* for three-dimensional visualization of crystal, volumetric and morphology data, J. Appl. Crystallogr. **44**, 1272 (2011).